

# On the Assembly of Dwarf Galaxies in Clusters and their Efficient Formation of Globular Clusters

Pouria A. Mistani<sup>1</sup> <sup>\*</sup>, Laura V. Sales<sup>1,2</sup>, Annalisa Pillepich<sup>2</sup>, Rubén Sanchez-Janssen<sup>3</sup>, Mark Vogelsberger<sup>4</sup>, Dylan Nelson<sup>2</sup>, Vicente Rodriguez-Gomez<sup>2</sup>, Paul Torrey<sup>4</sup> and Lars Hernquist<sup>2</sup>

<sup>1</sup>*Department of Physics and Astronomy, University of California, Riverside, CA, 92521, USA*

<sup>2</sup>*Harvard-Smithsonian Center for Astrophysics, 60 Garden Street, Cambridge, MA, 02138, USA*

<sup>3</sup>*NRC Herzberg Institute of Astrophysics, 5071 West Saanich Road, Victoria, BC, V9E 2E7, Canada*

<sup>4</sup>*Department of Physics, Kavli Institute for Astrophysics and Space Research, Massachusetts Institute of Technology, Cambridge, MA 02139, USA*

14 February 2022

## ABSTRACT

Galaxy clusters contain a large population of low mass dwarf elliptical galaxies whose exact origin is unclear: their colors, structural properties and kinematics differ substantially from those of dwarf irregulars in the field. We use the Illustris cosmological simulation to study differences in the assembly histories of dwarf galaxies ( $3 \times 10^8 < M_*/M_\odot < 10^{10}$ ) according to their environment. We find that cluster dwarfs achieve their maximum total and stellar mass on average  $\sim 8$  and  $\sim 4.5$  Gyr ago (or redshifts  $z = 1.0$  and  $z = 0.4$ , respectively), around the time of infall into the clusters. In contrast, field dwarfs not subjected to environmental stripping reach their maximum mass at  $z = 0$ . These different assembly trajectories naturally produce a color bimodality, with blue isolated dwarfs and redder cluster dwarfs exhibiting negligible star-formation today. The cessation of star-formation happens over median times 3.5–5 Gyr depending on stellar mass, and shows a large scatter ( $\sim 1$ –8 Gyr), with the lower values associated with starburst events that occur at infall through the virial radius or pericentric passages. We argue that such starbursts together with the early assembly of cluster dwarfs can provide a natural explanation for the higher specific frequency of globular clusters (GCs) in cluster dwarfs, as found observationally. We present a simple model for the formation and stripping of GCs that supports this interpretation. The origin of dwarf ellipticals in clusters is, therefore, consistent with an environmentally-driven evolution of field dwarf irregulars. However, the  $z = 0$  field analogs of cluster dwarf progenitors have today stellar masses a factor  $\sim 3$  larger—a difference arising from the early truncation of star formation in cluster dwarfs.

**Key words:** galaxies: dwarfs - galaxies: evolution - galaxies: interactions - galaxies: star clusters: general - methods: simulations

## 1 INTRODUCTION

By number, dwarf elliptical galaxies (dEs) dominate the population of dwarfs in cluster environments. They are, however, almost absent in the field, where the prevalent morphological type is gas-rich dwarf irregulars (dIrrs) (Binggeli et al. 1990; Grebel 1999; Geha et al. 2012). This difference immediately raises questions about the relationship between dEs and dIrrs. Are these two types of galaxies intrinsically different objects? Or, is there an evolutionary link between these two dwarf populations?

There is no strict definition for dE galaxies, but they are rather characterized by a combination of attributes such as having low mass, being of low surface brightness, and exhibiting red colors and low levels of star formation. Moreover, dEs have quite a heterogeneous morphological mix (Lisker 2009; Janz et al. 2012) and also show wide kinematic variations (Geha et al. 2002; van Zee et al. 2004a; Lisker 2006; Ryś et al. 2013; Toloba et al. 2014a,b). These observations hint at a complex formation scenario where more than one factor determines their final fate. Although the definition is not specific, there is clear consensus that dEs are less-disky and less rotationally-supported than dwarf irregulars in the field.

Differences between the two populations could arise from either internal or external mechanisms. It appears that dIrrs and dEs

<sup>\*</sup> E-mail: pakba002@ucr.edu

follow similar scaling relations, so they could be the same type of object but in which internal processes, like star-formation and feedback, caused some to retain more gas than others (Dekel & Silk 1986; de Rijcke et al. 2005). While appealing, such a scenario cannot explain the strong correlation observed with the environment. Alternatively, dEs may have been dIrrs in the past that were transformed into dEs later, due to environmental effects within their host clusters. Such a transformation could involve some degree of ram-pressure stripping and gas starvation to redden their colors (Conselice et al. 2003, van Zee et al. 2004b, Boselli et al. 2008), and tidal effects to heat them kinematically, altering their morphologies (Mayer et al. 2001; Gnedin 2003; Lisker 2009; D’Onghia et al. 2009; Smith et al. 2010; Lelli et al. 2014). A different and intriguing perspective for the influence of environment on dwarfs was argued by Sabatini et al. (2005), who noted that interactions with the cluster medium could temporarily *enhance* star formation in infalling dIrrs, leading to rapid consumption of the gas and a transformation into dEs. Finally, low mass dEs could also be the stripped remnants of more massive galaxies that fell into the cluster long ago (Conselice et al. 2003).

Environmentally driven transformation models for dEs, although attractive, are not free from challenges. One of the main problems with this scenario is the observed difference in the frequency of globular clusters (GCs) between dwarfs in clusters and in the field. If dEs and dIrrs are evolutionarily linked, dEs should contain similar or even fewer GCs than disk galaxies in the field because of tidal stripping within the cluster host. Instead, dEs in clusters tend to show an *increased* GC specific frequency over dIrrs at similar masses (Miller et al. 1998, Miller & Lotz 2007, Jordan et al. 2007b, Peng et al. 2008, Sanchez-Janssen & Aguerri 2012). This discrepancy appears accentuated for nucleated dEs (Miller & Lotz 2007) and dwarfs in the inner regions of clusters (Jordan et al. 2007b, Peng et al. 2008).

With their capability of being able to track the evolution of galaxies, numerical simulations could, in principle, resolve these issues. In practice, this is difficult because GC formation is still poorly understood cosmologically (however see an original attempt by Prieto & Gnedin 2008), and the dynamic range needed to self-consistently evolve dwarf galaxies with their GC systems in a galaxy cluster environment is currently prohibitive. Here, we propose a hybrid approach. Hydrodynamical simulations of a large cosmological volume are performed to enable us to sample a set of galaxy clusters and, simultaneously, to follow the assembly and evolution of dwarfs in clusters and in the field. In post-processing, we then apply a simplistic model of GC formation together with a particle-tagging technique to roughly describe the formation and stripping of GCs in cluster dwarfs. Our effort builds on the earlier work by Peng et al. (2008) based on semi-analytical catalogues and incorporates the effect of tidal stripping of GCs not addressed in their work.

This paper is organized as follows. We introduce the simulations and selection criteria for our samples in Sec. 2. The assembly of dwarfs according to their environment is investigated in Sec. 3 and the details of their star formation histories is presented in Sec. 4. We develop and apply our method for tracking GCs in Sec. 5, addressing the expected GC frequencies for cluster and field dwarfs. We summarize our main results in Sec. 6.

## 2 NUMERICAL SIMULATIONS

We employ a set of model galaxies taken from the Illustris Simulation (Vogelsberger et al. 2014a,b; Genel et al. 2014). Illustris consists of a cosmological box 106.5 Mpc on a side evolved with hydrodynamics using the code AREPO (Springel 2010). The simulation adopts a WMAP9-consistent cosmology and includes treatments of gravity together with the most relevant physical processes driving galaxy evolution, including gas cooling/heating (Katz et al. 1996; Faucher-Giguère et al. 2009), star-formation (Springel & Hernquist 2003), metal enrichment, and AGN feedback (Springel et al. 2005; Di Matteo et al. 2005; Sijacki et al. 2007). While a detailed description of the model can be found elsewhere (Vogelsberger et al. 2013), for completeness we briefly summarize the relevant aspects of the physics included in our simulations.

Gravity is computed using a Tree-PM approach in which long-range forces are calculated on a grid while short-range interactions are obtained by expanding the potential into multipoles (Springel 2005). The Euler equations governing the hydrodynamics of the gas are solved on an unstructured mesh that moves with the flow, yielding a continuously adaptive method to achieve high resolution where needed and simultaneously moderating the impact of numerical diffusion (Vogelsberger et al. 2012; Sijacki et al. 2012; Genel et al. 2013; Nelson et al. 2013). In this scheme, the gas is distributed among “cells”, which can be heated or cooled according to the local density and metallicity. Dense gas becomes eligible for star-formation above a density threshold  $n_H = 0.13 \text{ cm}^{-3}$ , at which point star particles are spawned probabilistically according to the local dynamical time.

We follow the evolution of stars, including mass and metal return from stellar winds and the explosion of massive stars (supernova type I and II; hereafter, SNI and SNII, respectively). In the case of SNII, we also consider the deposition of kinetic energy into galactic-scale winds, with initial velocities that vary linearly with the local velocity dispersion of the dark matter halo. The mass loading is then determined from the available energy from SNII explosions (Springel & Hernquist 2003). With these choices for the sub-resolution physics, the Illustris simulations have been shown to reproduce several of the observational properties of galaxies, such as their stellar mass and color distribution, morphological variety, angular momentum distribution and typical scaling relations, among others (Torrey et al. 2014; Genel et al. 2014, 2015; Snyder et al. 2015; Sales et al. 2015).

In the highest resolution run, or Illustris-1 (used here), the mass per DM and baryonic particle are  $m_{\text{DM}} \sim 6.26 \times 10^6 M_\odot$  and  $m_b \sim 1.26 \times 10^6 M_\odot$ , respectively. Gravity is softened with a spline kernel (Hernquist & Katz 1989) and the softening length scales with redshift but is always comparable to or better than  $\epsilon = 700(1400) \text{ pc}$  for the stellar (dark matter) particles. The most well-resolved gas elements can have extents as small as 48 pc.

Galaxies are identified as self-bound structures at each output using a combination of a Friends-of-Friends (FoF) algorithm (Davis et al. 1985) for groups and a subsequent application of the SUBFIND algorithm (Springel et al. 2001; Dolag et al. 2009). The centers are marked by the position of the particle with the minimum potential energy and galaxy properties are computed within twice the half-mass radius of the stars for each object. The time evolution of a given object is tracked by means of LHALOTREE merger trees (Springel et al. 2005; Nelson et al. 2015) from a total of 136 output snapshots covering the redshift range  $z = 50$  to  $z = 0$ .

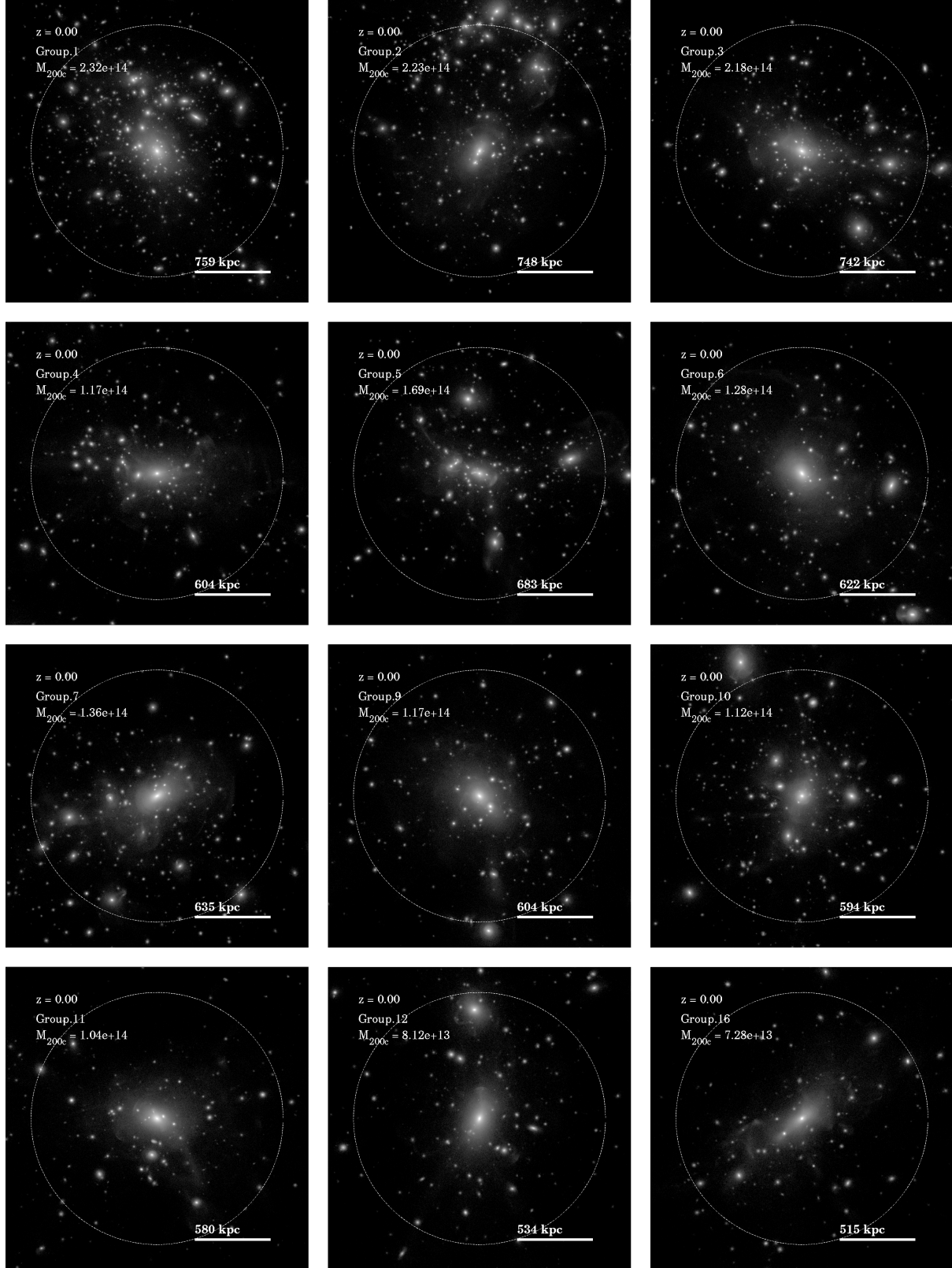


**Figure 1.** Projected stellar maps for the 12 most massive galaxy clusters in Illustris ( $M_{200} \geq 5 \times 10^{13} M_{\odot}$ ). Individual “clumps” correspond to satellite galaxies inhabiting each of the clusters. Circles indicate the extent of the virial radius.

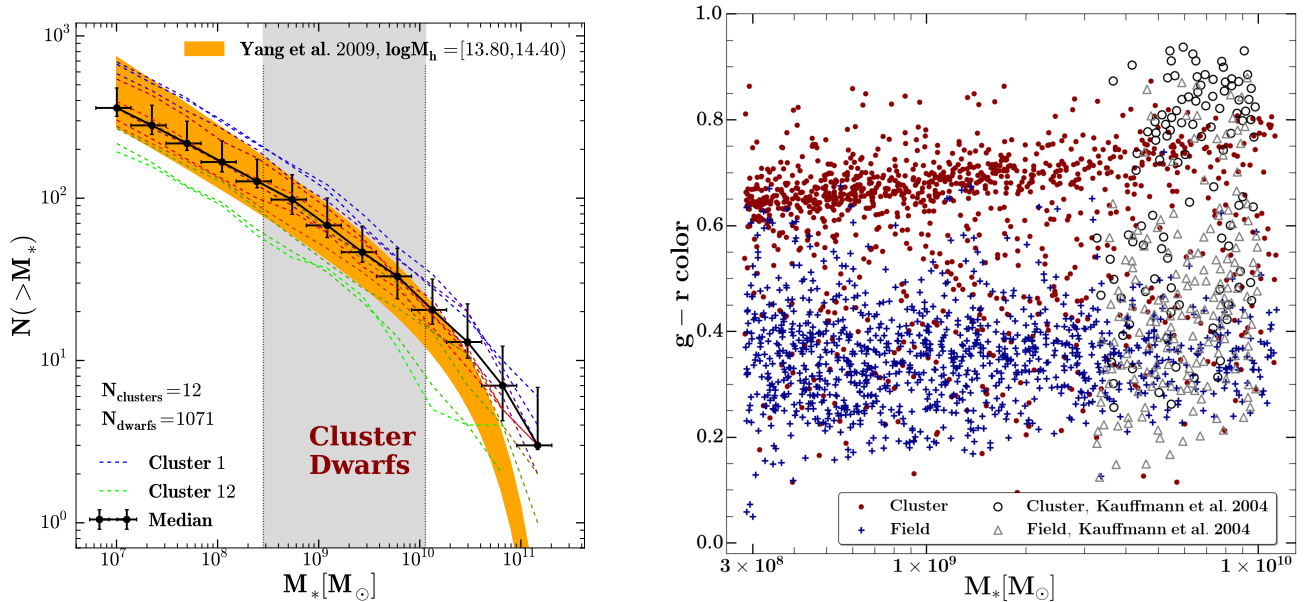


**Figure 2.** Left: Cumulative stellar-mass function of satellite galaxies for the simulated clusters in our sample. Individual clusters are shown with colored dashed lines and the median is indicated with solid black line/symbols. Our selection criteria for dwarf galaxies ( $M_* = [3 \times 10^8 - 1 \times 10^{10}] M_\odot$ ) is highlighted by the gray area. We find a total of 1071 cluster dwarfs. Note the good agreement with the SDSS observed satellite mass function (taken from Yang et al. (2009), orange shading), particularly in the selection region of our dwarfs. Right: The color-stellar mass distribution of dwarfs in our cluster sample (red dots) and field control sample (blue crosses), selected to be central (not satellites) objects in the same mass range. Encouragingly, cluster dwarfs are much redder than the field sample, as indicated by observations. We show in grey circles/triangles SDSS results for galaxies in low/high density environments taken from Kauffmann et al. (2004).

## 2.1 Simulated Dwarfs in Clusters and in the Field

Our sample of dwarfs consists of a set of “cluster” dwarfs selected to inhabit the most massive groups and clusters in *Illustris*, and “field” dwarfs, a control sample consisting of central low mass galaxies that are isolated. The selection is done once at  $z = 0$  and the time evolution of both populations is studied by following the progenitors of each object through time. To construct the cluster sample, we consider all galaxy clusters with virial mass  $M_{200} \geq 5 \times 10^{13} M_\odot$ , where the virial radius  $r_{200}$  is defined to be that which encloses 200 times the critical density of the Universe, and the virial mass  $M_{200}$  is the total mass contained within  $r_{200}$ . Applying these criteria, we obtain a total of 12 clusters, with the most massive reaching  $M_{200} = 2.32 \times 10^{14} M_\odot$ , similar to mass estimates for the Fornax (Jordan et al. 2007a) and the Virgo (Böhringer et al. 1994) galaxy clusters.

In Fig. 1 we show stellar density maps of the clusters in our sample, with the virial mass and original FoF-ID quoted in each panel. All clusters are populated by a large number of *satellite* galaxies, seen as individual “clumps” in each image, which cover a wide range of masses and properties. By definition, satellite galaxies are all objects identified by SUBFIND that are not the centrals of their FoF group.

The left panel of Fig. 2 shows the cumulative stellar-mass function of these satellite galaxies, indicated by colored dashed lines for each of the selected 12 clusters. We consider only satellites that are at  $z = 0$  within the virial radius of their host system. The median of our sample (black symbols/solid line) agrees well with

the satellite stellar-mass function of groups and clusters of similar mass in SDSS, as indicated by the orange shaded region (Yang et al. 2009). Cluster dwarf galaxies are then selected from these satellites by a simple mass cut,  $3 \times 10^8 < M_*/M_\odot < 1 \times 10^{10}$  (gray region), implying that all our dwarfs are resolved with at least 240 stellar particles today. This selection criterion yields a total of 1071 cluster dwarfs.

For comparison, we also define a sample of “field” dwarfs in the same stellar mass range but that are *central* galaxies of their FoF group (i.e. they are not satellites of any larger system). A total of 28391 dwarfs satisfy this condition, from which we randomly select 1071 to match the number of cluster dwarfs. Encouragingly, this simple selection procedure results in interesting differences between the color distributions of the “cluster” and “field” dwarf populations, as expected from observations of galaxies in different environments. The right panel of Fig. 2 shows that at fixed stellar mass, the cluster dwarfs (red dots) are significantly redder than the field objects (blue crosses), in good agreement with the observed redder colors of satellites around massive hosts (e.g., Dressler 1980; Martínez et al. 2002; Wang et al. 2014). This suggests that our simulation properly captures the main physical processes driving the evolution of galaxies in different environments and can therefore shed light on the formation and evolution of dEs in cluster environments.

## 3 THE ASSEMBLY OF DWARF GALAXIES IN DIFFERENT ENVIRONMENTS



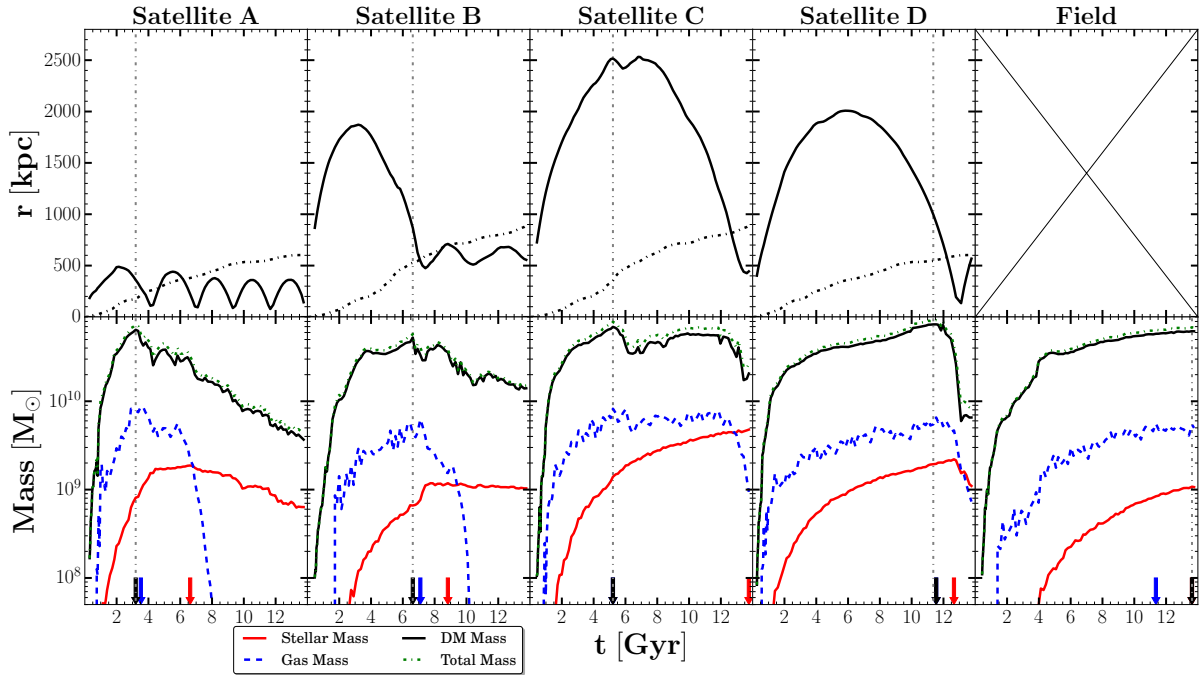


**Figure 3.** Examples of the orbits (top row) and mass evolution (bottom row) of cluster dwarfs (Satellites A-D) and a field dwarf (rightmost column). Orbits show a wide diversity, with some dwarfs completing more than 3-4 revolutions around the cluster (example Sat. A) and others only recently arriving (Sat. D). The time evolution of the host cluster’s virial radius  $r_{200}$  are indicated with a black dashed line in each panel. The time of maximum *total* mass (see green-dotted line in the bottom row) is indicated in all panels with a vertical dotted line. This time corresponds roughly to the moment they stopped being centrals to become satellites; which can happen right before crossing the virial radius of the cluster like in Sat. A, B and D, or before, if they were accreted into a smaller group first and then entered the cluster (like Sat. C). The mass evolution in the bottom row shows clear correlations with the orbits, with a decrease of mass after infall as well as close pericentric passages. Tidal stripping is not strong for the stellar component (solid red), although dwarfs in tightly bound orbits can experience significant stellar mass loss (example Sat. A). Small vertical arrows show the times at which each component (dark-matter, stars, gas) reaches its maximum. Stars continue to build up after infall, as shown by the shift between the dotted vertical line and the red arrows. Note that for field dwarfs, which are not exposed to stripping, the mass in all components peaks only at the present time.

The cluster dwarfs sample a wide variety of orbits around their central hosts. We show several examples in the top row and first 4 columns of Fig. 3. Dwarf satellites initially follow the Hubble expansion until they are captured by the gravitational field of a cluster and then turn around (seen as the moment of maximum distance from the cluster). They then begin the process of infall and settle into their orbits around the host potential. Some dwarfs in our sample have fallen in more than 10 Gyr ago, completing several revolutions around the cluster’s center by the present (e.g. Satellite A). On the other hand, some objects have only recently been accreted into the cluster (Satellite D), crossing the host virial radius less than 2 Gyr ago (the time evolution of the host virial radius is shown with a dashed line). From this perspective, the sample of cluster dwarfs is a complex group of objects whose properties are expected to be diverse in light of the variations present in their orbital histories.

Orbits have a clear impact on the mass evolution of cluster dwarfs, as shown in the bottom row of Fig. 3. Dwarfs initially grow as expected (green dotted line shows the evolution of total mass) but they later reach a maximum after which their total mass decreases due to tidal stripping. The maximum is usually reached at the last time the dwarfs are the central object of their FoF group. Therefore, this time of maximum mass, shown as vertical dotted lines in each panel, is a good indicator of the time of infall, or the time when dwarfs stopped being central objects to become satellites. In what follows, we will refer to the time of infall  $t_{\text{inf}}$  or infall redshift  $z_{\text{inf}}$

as the time when the simulated dwarfs reached their maximum total mass  $t_{\text{max}}$ .

There are two interesting points to notice from these growth curves. Some dwarfs (e.g. Satellite C) first become a satellite of a different system that later fall into the cluster. This pre-processing of dwarfs is not uncommon, and is usually accompanied by a wiggly pattern in their orbits as they move around a different host on the way to their final infall into the cluster (see Satellite C around  $t \sim 5.5$  Gyr). Pre-processing effects in groups have been hypothesized to account for the observed properties of the Magellanic Clouds (Besla et al. 2007, 2010, 2012), and is also expected to happen regularly in cluster dwarfs (e.g. Lisser et al. 2013). For our sample, 65% of the objects infall first into an intermediary system, where they spend a rather short amount of time (median of  $\sim 1.3$  Gyr), before finally infalling into their host galaxy clusters where they stay until  $z = 0$ . Second, the small difference between the green dotted and black solid lines suggests that stripping mainly affects the dark matter component (solid black line). The times when the maximum total mass  $t_{\text{max}}$  and maximum dark matter mass  $t_{\text{max}}^{\text{DM}}$  are reached always track one another (see black arrows).

Baryons, instead, show a different behaviour. Stars are much more centrally concentrated than the dark matter component, resulting in a small fraction of the stellar mass being tidally stripped (with some exceptions as in Satellite A). In our sample of 1071 cluster dwarfs, 62% retain more than 80% of their maximum stel-

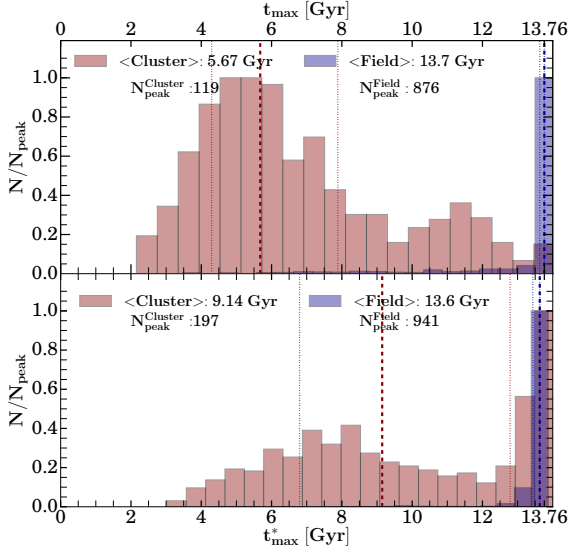


**Figure 4.** Distributions of the time of maximum *total* mass  $t_{\max}$  (top) and maximum *stellar* mass  $t_{\max}^*$  (bottom). Histograms are normalized to the peak value in each sample (values quoted). Cluster/Field dwarfs are shown in red/blue. Due to stripping, dwarfs in clusters assemble their mass earlier, typically reaching their maximum mass at  $t_{\max} \sim 5.5$  Gyr or  $z \sim 1$ , unlike the field population which continues to grow until today ( $t_{\max} \sim 13.7$  Gyr). The time of maximum *stellar* mass in cluster dwarfs is about 3.5 Gyr later than the time of maximum *total* mass, indicating that satellite dwarfs can continue to form stars for a significant period of time after they have become satellites.

lar mass and only 1% have lost more than 90% of their stars by  $z = 0$ . For comparison, this corresponds to 2% and 18% objects respectively for the same thresholds in the dark matter component. Moreover, the stellar mass continues to grow after dark matter stripping has begun, as indicated by the red arrows marking the time of maximum stellar mass for each object,  $t_{\max}^*$ . This agrees well with previous findings in Illustris of significant star formation continuing after satellite infall (Sales et al. 2015; Rodriguez-Gomez et al. 2015). The gaseous component (dashed blue line) stops growing around the time of infall and tends to be equally or more greatly affected by the environment than the dark matter component. Tidal stripping as well as gas consumption from star formation and hydrodynamical effects like ram-pressure stripping contribute to this effect. Most cluster dwarfs (74%) show significant gas depletion, losing more than 90% of their maximum gas mass, which is consistent with the low levels of star-formation driving the red colors seen previously in Fig. 2.

The evolution of dwarfs in the field is remarkably different. The last column in Fig.3 shows the mass evolution of a random dwarf from the field sample. Of note, all components show a steady mass growth until  $z = 0$ , with occasional pronounced mass-gain events associated with mergers (for example at  $t \sim 4$  Gyr). Galaxies in the field do not experience significant stripping, and therefore, reach a maximum mass at the present day, as shown by the vertical dotted line and small arrows. This is not a feature of this particular dwarf, but rather the norm in the whole field dwarf sample, as shown in Fig.4. The top panel shows the distribution of  $t_{\max}$  (the times when the total maximum mass is reached) for all cluster (red) and field (blue) dwarfs. The median and 25%-75% percentiles are shown as vertical dashed and dotted lines, respectively. For most

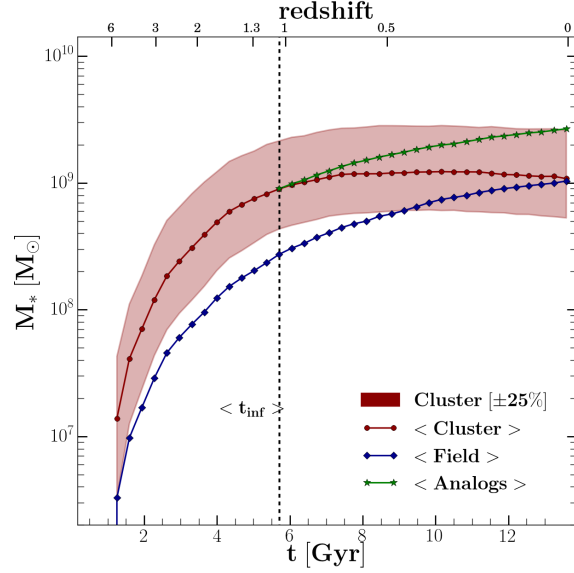


**Figure 5.** Median stellar mass evolution for the sample of cluster (red) and field (blue) dwarfs. The 25%-75% dispersion on the median is shown as the shaded area for the cluster dwarf sample only, but is of similar magnitude for the field dwarfs. Although both samples have (by construction) the same mass at  $z = 0$  their time evolution is significantly different: cluster dwarfs were more massive than the field sample at earlier redshifts. Both samples gain mass at approximately the same rate up to  $z \sim 1$ , when the growth of cluster dwarfs decelerates due to environmental effects (median infall time of the sample shown by the vertical dashed line). In contrast, a sample of dwarf analogs that had the same properties as the progenitors of cluster dwarfs at the time of infall (instead of at  $z=0$ ) would outgrow the median stellar mass in cluster dwarfs by up to a factor  $\sim 3$  today (green line).

dwarfs in the field,  $t_{\max} \sim 13.7$  Gyr (i.e., ‘today’) whereas the median for cluster dwarfs is  $t_{\max} \sim 5.6$  Gyr or  $z = 1.1$ . A similar behaviour is seen for the time of maximum stellar mass, with field dwarfs assembling their stars significantly later than their cluster counterparts ( $t_{\max}^* \sim 13.6$  and  $9.14$  Gyr for field and cluster dwarfs respectively). Fig. 4 highlights that a significant level of star formation after infall is a common feature for cluster dwarfs (the median  $t_{\max}$  and  $t_{\max}^*$  differ for more than  $\sim 3$  Gyr); a subject we will return to in Sec. 4.

This different stellar mass assembly can be better appreciated from Fig. 5 for the population of cluster (red) and field (blue) dwarfs. Curves correspond to the median of the samples, and the 25%-75% dispersion is indicated by the shaded region (for clarity only shown for the cluster dwarfs but is of similar magnitude for the field objects). Because of our selection, the curves overlap at  $z = 0$  where both samples were chosen to be within the same stellar mass range:  $3 \times 10^8 < M_*/M_\odot < 1 \times 10^{10}$ . However, going back in time, the samples diverge. Field dwarfs form their stars steadily throughout their history up to  $z = 0$ . In contrast, dwarfs in clusters grow their mass rapidly at early times, then being 3-4 times more massive than the field sample. However, by the median time of infall of the cluster sample,  $\langle t_{\text{inf}} \rangle \sim 5.5$  Gyr (vertical dashed line), the stellar mass freezes and does not appreciably change thereafter. This behaviour is caused by more dwarfs becoming satellites, lowering their star-formation rates and being exposed to tidal stripping.

This excess of mass at early times with respect to today’s field

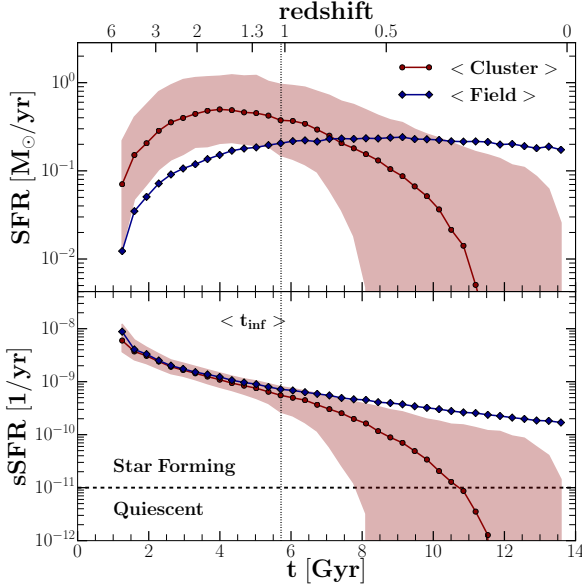


**Figure 6.** Median star formation rate (SFR, top panel) and the specific star formation rate (sSFR, bottom panel) as a function of time for cluster (red) and field (blue) dwarfs. Color coding is the same as in Fig. 5. Dwarfs in clusters form their stars at higher SFR than the field sample. However, the difference is only due to their larger stellar mass at high redshifts, since the sSFR of both samples agrees well before the average time of infall  $\langle t_{\text{inf}} \rangle \sim 5.5$  Gyr. After that, the median rate of star formation in cluster dwarfs decreases, with most objects becoming quiescent by  $z = 0$ . We define  $\text{sSFR} = 10^{-11} \text{ yr}^{-1}$  as our threshold to divide star-forming from quiescent objects (black dashed line).

objects suggests that, if they were in the field, cluster dwarfs would have grown significantly more in mass by today. Processes associated with the cluster environment have truncated that growth. We examine this possibility by defining a group of cluster dwarf “analogs” (green line), selected to have similar mass as the cluster dwarfs at time of infall but that, unlike the cluster dwarfs, remain isolated field objects until the present<sup>1</sup>. This exercise shows that a sample selected to match cluster dwarfs at infall rather than at  $z = 0$  ends up a factor  $\sim 2.5 - 3$  more massive on average than the cluster dwarfs today. The most appropriate comparison sample is thus unclear and may depend on the question being addressed. Our results indicate that selecting isolated objects in the field having  $\sim 3$  times more mass than the cluster dwarfs we are targeting may provide a better match to the early phases of growth of both samples. To facilitate the comparison with observations, in what follows we will still consider our “field” objects selected within the same mass range as cluster dwarfs at  $z = 0$  to be the control sample, but we bear in mind the lesson learned from the “analogs” sample.

<sup>1</sup> In practice, the selection of “analogs” is done as follows: at the median infall time of the cluster dwarfs sample  $\langle z \rangle \sim 1.1$ , we select all field objects that at that time have a stellar mass within a factor of 2 of the median stellar mass of the progenitors cluster dwarfs at the same time. We then follow the selected objects forward in time to identify those that remain central galaxies to  $z = 0$  and choose 1071 objects randomly from that set.

#### 4 THE STAR FORMATION HISTORY OF DWARF GALAXIES: CLUSTER VS. FIELD

We now turn our attention to *how* dwarfs form their stars according to their environment. Fig. 6 shows the median star formation rate (SFR, upper panel) and specific star formation rate (sSFR, lower panel) of our samples as a function of time. We define the sSFR as the SFR divided by instantaneous stellar mass of the galaxy. As before, red/blue corresponds to cluster/field dwarfs and 25%-75% percentiles are indicated by the shadowed region. As expected from the mass difference seen in Fig. 5, cluster dwarfs form stars at a higher rate than in the field at early times, but the trend reverses as more dwarfs become satellites after  $z = 1$ . By the present day, the vast majority of cluster dwarfs have stopped forming stars, consistent with the red colors displayed in Fig. 2. Interestingly, the SFR difference at high redshifts is only due to the different masses of the samples: once the SFR of each dwarf is normalized by their (instantaneous)  $M_*$ , the specific rates between the samples are consistent with each other (bottom panel). Cluster dwarfs are not “special” objects in this regard and simply form stars according to the expected rate given their stellar mass.

Beyond averaging the samples, examination of individual star formation histories of dwarfs reveals another interesting aspect of cluster dwarfs. Fig. 7 shows the SFR evolution corresponding to Satellites A-D and the field dwarfs shown in Fig. 3. The curves in the first three panels show significant peaks or “bursts” of star formation that are not present in the field objects or in Satellite D. Such bursts, when present, seem to occur around the time of infall (indicated by the vertical dotted line) and we have checked that these events are usually associated with either the crossing of the virial radius of the cluster or to the time of first pericentric passage. Often times the star formation is quenched immediately following this final “burst”.

We would expect that the tidal and ram-pressure interactions with a cluster could trigger a compression of the interstellar medium of a cluster dwarf, temporarily raising its star formation rate. Such an effect has previously been seen in idealized simulations (Barnes & Hernquist 1996; Mihos & Hernquist 1996; Mayer et al. 2001). Here we find that the triggering of short “bursts” of star formation by the environment should be quite common among dwarfs in clusters today. Additionally, we have explicitly checked that mergers with other galaxies *within* the clusters are far too infrequent to be responsible for the measured star formation increase in cluster dwarfs. At any given time, satellite dwarfs have a median merger rate at least  $\sim 1$  dex below that of the field counterparts.

We quantify the presence of bursts of star formation by measuring the standard deviation of the SFR at each snapshot with respect to the time-average:

$$\sigma_{\text{SFR}} = \frac{\sqrt{\Sigma(\text{SFR}(t) - \overline{\text{SFR}})^2 / N_t}}{\overline{\text{SFR}}}, \quad (1)$$

where  $N_t$  is the number of time points where we measure the SFR (i.e., the number of output snapshots of the simulation), and  $\overline{\text{SFR}}$  is the time averaged SFR from all snapshots (indicated with a cyan curve in each panel of Fig. 7). Values for  $\sigma_{\text{SFR}}$  are quoted for all

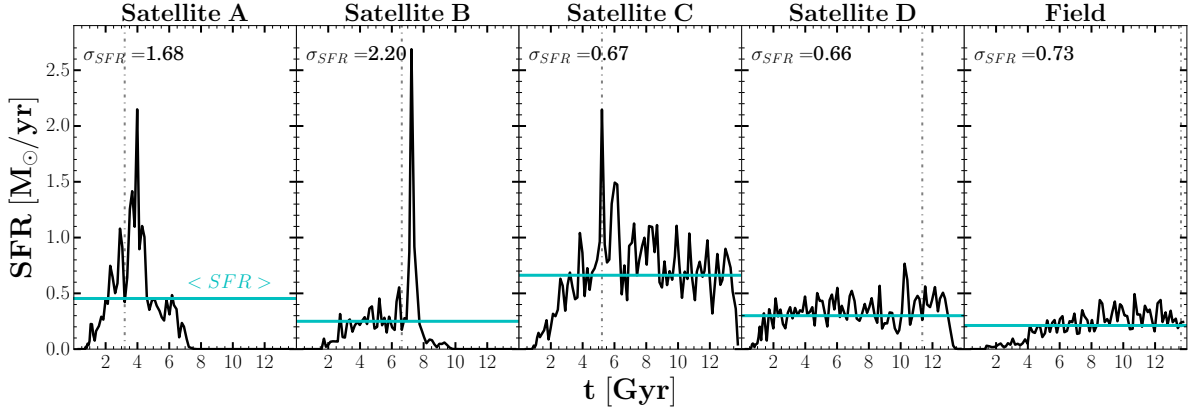


**Figure 7.** Examples of individual star formation histories for the same satellite and field dwarfs in Fig. 3. As in the case of the orbits, the SFR histories of cluster dwarfs exhibit large variations. It is not uncommon to see “peaks” or episodes of intense star formation (for example Sat. A, B) that coincide with the crossing of the virial radius of the cluster and/or first pericentric passages. Starburst events are not common for field dwarfs. Some cluster dwarfs show a more constant SFR that is comparable to field objects (for example Sat. D). In each panel, we quote the “starburstiness” of the curve,  $\sigma_{\text{SFR}}$ , defined as the standard deviation of the SFR history with respect to the time-average  $\langle \text{SFR} \rangle$  (cyan line). Large values of  $\langle \text{SFR} \rangle$  indicate the presence of starbursts. (See text for more details.)

dwarfs in Fig. 7 and they appear to correlate well with the visual intuition of “burstiness” in each curve<sup>2</sup>.

Fig. 8 extends the trend hinted by these 5 individual examples to all dwarfs in our samples. We show  $\sigma_{\text{SFR}}$  for cluster (red & orange dots) and field (blue crosses) dwarfs, plotted as a function of the local density  $\delta$  (where  $\delta$  is defined as the galaxy overdensity within the radius that encloses the 5th nearest neighbour, and only galaxies with  $r$ -band magnitude brighter than  $-19.5$  are used to compute the density field). Not only do field and cluster dwarfs separate cleanly in environment (as expected), they also show very different distributions of  $\sigma_{\text{SFR}}$ . Cluster dwarfs typically have larger  $\sigma_{\text{SFR}}$  values, indicating the presence of significant peaks or starburst events in their star-formation histories.

Moreover, green dots/histogram in Fig. 8 show the “analogs” sample described in Sec. 3 (selected to have similar progenitor masses as cluster dwarfs at time of infall). This sample is also characterized by low  $\sigma_{\text{SFR}}$  values alike the field galaxies, confirming that SFR enhancements in cluster dwarfs are purely associated to environmental effects and is not a bias in their progenitor mass. Although the trend with environment is weak above the field-cluster threshold, dwarfs in the very inner regions of clusters show even larger  $\sigma_{\text{SFR}}$  compared to the rest of the satellites (the orange histogram includes only satellite dwarfs that are today within  $0.5r_{200}$ ). *Our results indicate that cluster dwarfs, particularly those in the inner parts of clusters today, likely had a more “bursty” star formation history than dwarfs in the field.*

Star formation in satellite galaxies is expected to be truncated sometime after infall. Because the time-scale for this to occur sheds valuable information on the mechanisms responsible for this quenching (and how it may depend on host and satellite properties), the subject has received significant attention from the community (e.g., Wang et al. 2007; Font et al. 2008; Wetzel et al. 2013;

Wheeler et al. 2014; Fillingham et al. 2015). In Fig. 9 we consider the time elapsed between infall and “quenching”, defined as the first time a dwarf’s SFR drops below  $\text{sSFR} \approx 10^{-11} \text{ yr}^{-1}$ . This threshold was chosen to be compatible with the definition in Wetzel et al. 2013, and we have additionally confirmed that it applies to the scale of dwarfs by checking that it is always 2 dex below the average sSFR of dwarf centrals at any given time. For cluster dwarfs, we show the quenching time as a function of satellite mass, where dots correspond to our simulated dwarfs that are quiescent by  $z = 0$  (cluster dwarfs that are still star-forming today do not appear in this plot; they amount to  $\sim$  a third of the sample).

Interestingly, we find a positive trend with mass: the quenching timescale increases with the stellar mass from a median of  $\sim 3$  Gyr for our smallest objects to  $\sim 5.5$  Gyr at  $M_* = 10^{10} M_\odot$  (solid dark red curve). Notice that the scatter about this mean trend is significant, comfortably spanning the range  $\sim 1$ -8 Gyr after infall. Moreover, the dispersion is not random, but appears to correlate strongly with the mode of star formation, as quantified by  $\sigma_{\text{SFR}}$ : dwarfs with significant “burstiness” (large  $\sigma_{\text{SFR}}$  values) preferentially show shorter time-scales for quenching than objects with a lower  $\sigma_{\text{SFR}}$  at a given stellar mass (see color-coding). Long quenching time-scales are associated with dwarfs that passively consume their gas while rapid quenching is often triggered by a last burst of star formation that consumes all available fuel for the formation of stars.

Comparing these results to observational data is not straightforward. Samples of groups/clusters are typically not complete down to the masses of the dwarf galaxies studied here. On the other hand, the properties of dwarf galaxies in this mass range are well-studied in the Local Volume, where they are easier to observe due to their faint luminosities, or around  $\sim L_*$  isolated primaries where statistics are better for the hosts compared to more massive groups and clusters. Although not ideal, we attempt to put our results in the context of available observations in Fig. 9.

We start by comparing with the quenching time-scales in clusters but for more massive galaxies than our dwarfs (where there is observational data). For this, we extended our analysis to all satellite galaxies in the 12 simulated cluster hosts in Illustris. We select all surviving satellites at  $z = 0$  that are within the virial radii of our

<sup>2</sup> We have explicitly checked the robustness of  $\sigma_{\text{SFR}}$  by first smoothing the curves with a Savitzky-Golay filter of width  $t = 0.5 - 1$  Gyr. Since all measures seem to correlate well with the unfiltered version we decided to use the data without the smoothing, since the filtering introduces an arbitrary time-scale that is in principle unknown and could vary from dwarf to dwarf.



clusters and define their quenching time-scales in the same way as earlier. The median values obtained are indicated with the dark red dashed curves in Fig. 9. For such massive satellites, we overplot observational estimates from [Wetzel et al. \(2013\)](#) using SDSS data. The agreement is good, as shown by the solid red/green curves that bracket our host halo masses. Unfortunately, this does not guarantee that the time-scales for lower mass dwarfs in the simulations is reasonable; but it is reassuring that the model is similar to the observational data in the mass range where they overlap.

A closer look at Fig. 9 reveals a preferred mass around  $M_* \sim 8 \times 10^9 M_\odot$  where this quenching timescale is maximum, indicated by the medians in solid and dashed dark red curves. The reason for this upturn is unclear, but is likely connected to the physical mechanisms quenching these galaxies; we defer to a detailed study of this in a companion paper ([Mistani et al., in-prep](#)). The timescales for our  $M_* \sim 10^9 M_\odot$  objects seem short compared to similar mass objects observed around  $L^*$  galaxies (data taken from SDSS data in [Fillingham et al. \(2015\)](#) and [Wheeler et al. \(2014\)](#)); however the comparison is inconclusive, as we cannot rule out a dependence on host halo mass on this scales. A more detailed comparison awaits until observational constraints on the quenching of dwarfs in clusters become available.

Summarizing, our results indicate that the star formation histories of cluster and field galaxies –with similar stellar mass today– differ: cluster dwarfs form their stars earlier, at higher star-formation rates and with occasional starbursts as they orbit their host cluster. In contrast, field dwarfs form their stars at later times and with typically lower SFRs. This clearly leaves an imprint in the stellar populations of these two sets of dwarfs, explaining the much redder colors in the cluster dwarfs compared to objects in the field. Could these different star formation histories also leave an imprint in the globular clusters populations of dwarfs? We investigate this in the following Section.

## 5 IMPLICATIONS FOR THE EXCESS OF GLOBULAR CLUSTERS IN DWARF ELLIPTICAL GALAXIES

There is not a clear picture for how globular clusters (GCs) form, but their properties are consistent with being the evolved versions of the young star clusters that are found in nearby star-forming galaxies ([Ho & Filippenko 1996](#); [Mengel et al. 2002](#); [de Grijs et al. 2004](#)). For example, the GC population of dwarfs in the Local Volume appears consistent with the initial mass function of young stellar clusters, after accounting for stellar and tidal evolution ([Kruijssen & Cooper 2012](#)). Therefore we consider the possibility that the processes and physical conditions behind the formation of today’s GCs are the same than those driving the formation of young star clusters at  $z = 0$ .

Analytical arguments suggest that gas-rich, high-pressure environments offer the most propitious conditions for the formation of bound star clusters ([Harris & Pudritz 1994](#); [Elmegreen & Efremov 1997](#); [Shapiro et al. 2010](#); [Kruijssen 2012](#)); a claim that has also found support from numerical simulations ([Kravtsov & Gnedin 2005](#); [Bournaud et al. 2008](#); [Renaud et al. 2008](#)). Observationally, there is strong evidence in favour of a link between star cluster formation and local properties of the interstellar medium. In particular, the fraction of stars born in clusters (that survive the

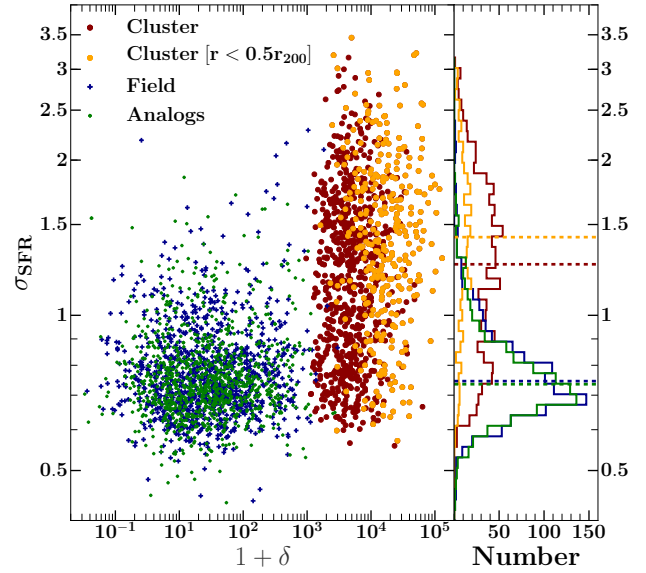


**Figure 8.** Measurement of “starburstiness” in SFRs of dwarf galaxies (quantified by means of  $\sigma_{\text{SFR}}$ ) as a function of the galaxy density of the local environment  $\delta$ . Large  $\sigma_{\text{SFR}}$  are associated with the presence of starbursts. Field dwarfs (blue crosses) inhabit less dense environments and show lower  $\sigma_{\text{SFR}}$  values compared to cluster dwarfs (red circles). The early “analogs” of cluster dwarfs (green symbols) also show low  $\sigma_{\text{SFR}}$  consistent with field objects. Histograms on the right show the distribution of  $\sigma_{\text{SFR}}$  for both samples together with the median indicated by dotted lines. Starbursts are more common among cluster dwarfs, particularly those that are today in the densest inner regions of clusters (orange distribution corresponds to cluster dwarfs within  $r < 0.5r_{200}$  today).

embedded phase) compared to the total amount of stars formed, termed  $\Gamma$ , appears to correlate with the density of star formation as ([Goddard et al. 2010](#)):

$$\Gamma = 0.29 \left( \frac{\Sigma_{\text{SFR}}}{M_\odot \text{yr}^{-1} \text{kpc}^{-2}} \right)^{0.24}, \quad (2)$$

with  $\Sigma_{\text{SFR}}$  defined as the averaged projected density of star formation in a galaxy. Such a scaling was later confirmed by other independent studies ([Adamo et al. 2010](#); [Silva-Villa & Larsen 2011](#); [Adamo et al. 2011](#)). If indeed star clusters form at the high density tail of the interstellar medium ([Kruijssen 2012](#)), then it is expected that GC formation was more efficient at higher redshifts (when galaxies were typically more gas-rich and turbulent) and during starburst events; interestingly this corresponds to two of the main differences in the star formation histories of our cluster dwarfs compared to our field galaxies.

To address this issue in some detail and to roughly predict the GC efficiencies in cluster and field dwarfs, we implement a simple model for the formation of GCs as a post-processing algorithm in our simulations. The model involves three steps: *i*) compute the amount of stellar mass born in star clusters, *ii*) sample an initial mass function of clusters and *iii*) use a particle tagging scheme to address the tidal removal of GCs from dwarfs orbiting inside galaxy clusters.

For the first step, we use the empirical relation from [Goddard et al. \(2010\)](#), where for each dwarf at a given time we compute

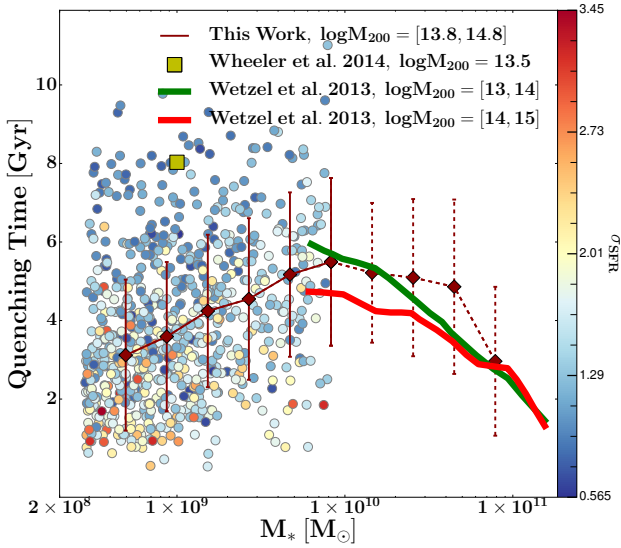


**Figure 9.** Quenching time-scales for dwarfs in clusters as a function of stellar mass, where the time-scale is defined as the difference between infall time and the time at which the sSFR drops below  $10^{-11} \text{ yr}^{-1}$ . Cluster dwarfs are shown with circles color coded by their  $\sigma_{\text{SFR}}$ . The median quenching time increases with stellar mass (red solid line). Interestingly, the dispersion around this median is large but is well-correlated with the *mode* of star formation: starbursts events (large  $\sigma_{\text{SFR}}$ ) are associated preferentially with the shortest timescales at a given stellar mass. To compare with observations, we extend this analysis to satellite galaxies in clusters but that are more massive than our dwarfs (median and dispersion shown with red dashed lines). These agree well the time-scales derived for SDSS galaxies in Wetzel et al. 2013 (red/green lines) for this mass range. The black square shows the inferred quenching time-scale for  $10^9 M_{\odot}$  dwarfs orbiting around  $L_*$  isolated primaries.

the fraction of stars formed that are born in bound clusters using Eq. 2. We define  $\Sigma_{\text{SFR}}$  as the sum of the star formation of all gas cells in the galaxy and we divide by the area of a circle with radius equal to that enclosing 95% of the star-forming gas (a good proxy for the  $H_{\alpha}$  radius). We then repeat this calculation throughout the time evolution of each dwarf, averaging in time-steps of 1 Gyr (we have explicitly checked that the results do not depend on the time window used). Adding up the mass in stars that is born in clusters for each of the time-steps gives us a prediction for the total mass expected in star clusters for each dwarf.

Fig. 10 shows the distribution of the computed mass in GCs for the population of cluster (red) and field (blue) dwarfs. Although the distributions overlap, we find a significant difference between the two, with cluster dwarfs having on average a factor  $\sim 2$  times more stellar mass in bound clusters than field dwarfs (vertical lines show the median in each sample). The difference is largely due to the earlier and higher SFRs in the former, as discussed in Sec. 4. This overall trend is in good agreement with results from the semi-analytical models presented in Peng et al. (2008), but the star-formation histories of field and cluster dwarfs are much more alike in their model (based on the Millennium simulations plus Guo et al. (2011) semi-analytical catalog) than in our sample.

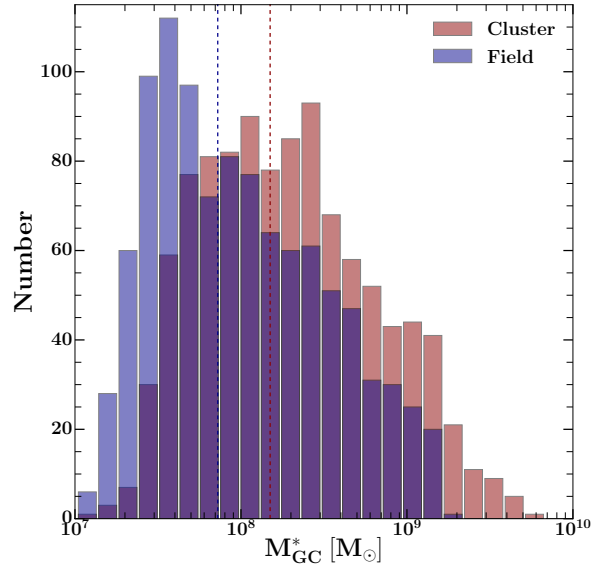


**Figure 10.** Mass in GCs predicted for the field (blue) and cluster (red) dwarf samples according to our post-processing model of GC formation (see Sec. 5). Although the distributions overlap, dwarfs in clusters have on average  $\sim 2$  times more mass in GCs than the field dwarfs; an effect dominated by the earlier and more bursty star-formation in cluster dwarfs.

In order to compare more closely with observational measurements of the GC efficiency in dwarfs, we need to translate our estimates of mass in GCs to GC numbers. Following Jordan et al. (2007b), we assume a Schechter-like cluster mass function and randomly sample from such a distribution until we account for the total GC mass for each dwarf. In particular, we adopt:

$$\frac{dN}{dM} \propto M^{-2} \exp(-M/M_c), \quad (3)$$

where  $M_c = 2 \times 10^5 M_{\odot}$  is the truncation mass. For our study, we focus on the high mass end, where GCs are more resilient to destruction by internal and environmental mechanisms. We sample globular clusters in a mass range of  $[1 \times 10^4 M_{\odot}, 1 \times 10^8 M_{\odot}]$ , where the upper bound is set to ensure that GCs have less mass than the galaxy itself. This is in general not important, as the rapid fall-off of the Schechter function ensures that high-mass clusters are highly uncommon. Notice that the low mass end we choose for the sampling works as a “normalization” factor to our total number of GCs (if we choose a smaller mass, we get a higher number of GCs and the same mass can now be distributed among many smaller-mass GCs than before). Thus, in what follows, our results are *differential* between both the dwarf samples. Our main aim is to compare the results for the cluster and field samples with respect to each other under the same assumptions.

For dwarfs in the field, this is enough to compute their GC specific frequency  $T_N$ , defined as the number of GCs divided by the stellar mass of the dwarf,  $T_N = N_{\text{gc}}/M_*/10^9 M_{\odot}$  (Zepf & Ashman 1993). However, for dwarfs in clusters, the tidal forces exerted by the host cluster potential can potentially strip some of the GCs originally formed in-situ. We therefore implement a particle-tagging technique, where we “paint” GCs on some dark-matter particles and use those particles as tracers of the time evolution for the

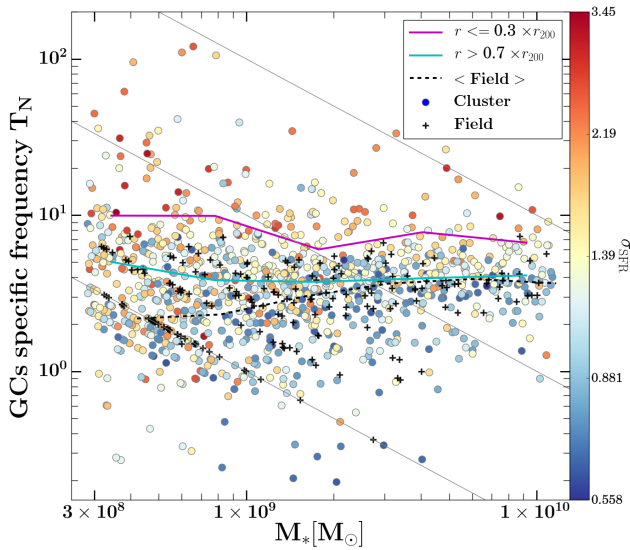


**Figure 11.** Final specific frequency of GCs for the sample of dwarfs in clusters (colored circles) and in the field (black crosses).  $T_N$  is computed as the number of GCs within an aperture of 8 kpc divided by the stellar mass of each object.  $T_N$  also accounts for the effects of environmental tidal stripping. In agreement with observations, we find that cluster dwarfs have a larger frequency of GCs than field dwarfs of the same  $M_*$ , a trend that is enhanced for dwarfs with starburst star formation histories (higher  $\sigma_{\text{SFR}}$ , see color coding) and/or dwarfs in the inner regions of clusters. Magenta and cyan lines show the medians for cluster dwarfs with  $r < 0.3r_{200}$  and  $r > 0.7r_{200}$ , respectively; field dwarfs shown with dotted black line. (For clarity, we only show 1 in 5 field dwarfs selected randomly from the sample.) Inclined grey lines show lines of constant number of GCs: 100, 10 and 1 from top to bottom. Differences are *relative* between the field and cluster samples, as the vertical normalization is chosen to coincide roughly with observed  $T_N$  range (see text for more detail).

GC population. This technique is not dynamically self-consistent (the mass of the dark-matter particle does not coincide with the GC that was “painted” onto it) but the expected error is small. The technique has been successfully used before in studies of GCs (Griffen et al. 2010; Ramos et al. 2015), stellar halos (Cooper et al. 2010, 2013), brightest cluster galaxies (Napolitano et al. 2003; Laporte et al. 2012; Cooper et al. 2015), and structure of dwarf spheroidal galaxies (Peñarrubia et al. 2008), among others.

For our tagging technique, we randomly select particles following a steep density profile,  $\rho_{\text{GC}} \propto r^{-3.5}$ , which is consistent with the distribution of GCs around the Milky Way according to the GC catalog in Harris (1996). We use a maximum distance equal to 10 kpc, but the steep slope ensures that the half-number radius is only 1–2 kpc, in agreement with observations of dwarfs (Georgiev et al. 2009). Our results do not depend on this maximum radius assumed. For each cluster dwarf, the tagging in time is done only once, at  $t_{\text{max}}$ . Although some of the star clusters will continue to form after infall into the galaxy cluster, we assume that the total number of GCs is already in place at the time of infall, which simplifies the procedure compared to tagging particles at individual time-steps. This approach is conservative, as tagging particles at an earlier time can only increase the chances of stripping later on.

After the particles have been selected at  $t_{\text{max}}$  for each dwarf, we use their IDs to check for their positions at  $z = 0$  and consider the GCs as bound/stripped according to their distance to the dwarf

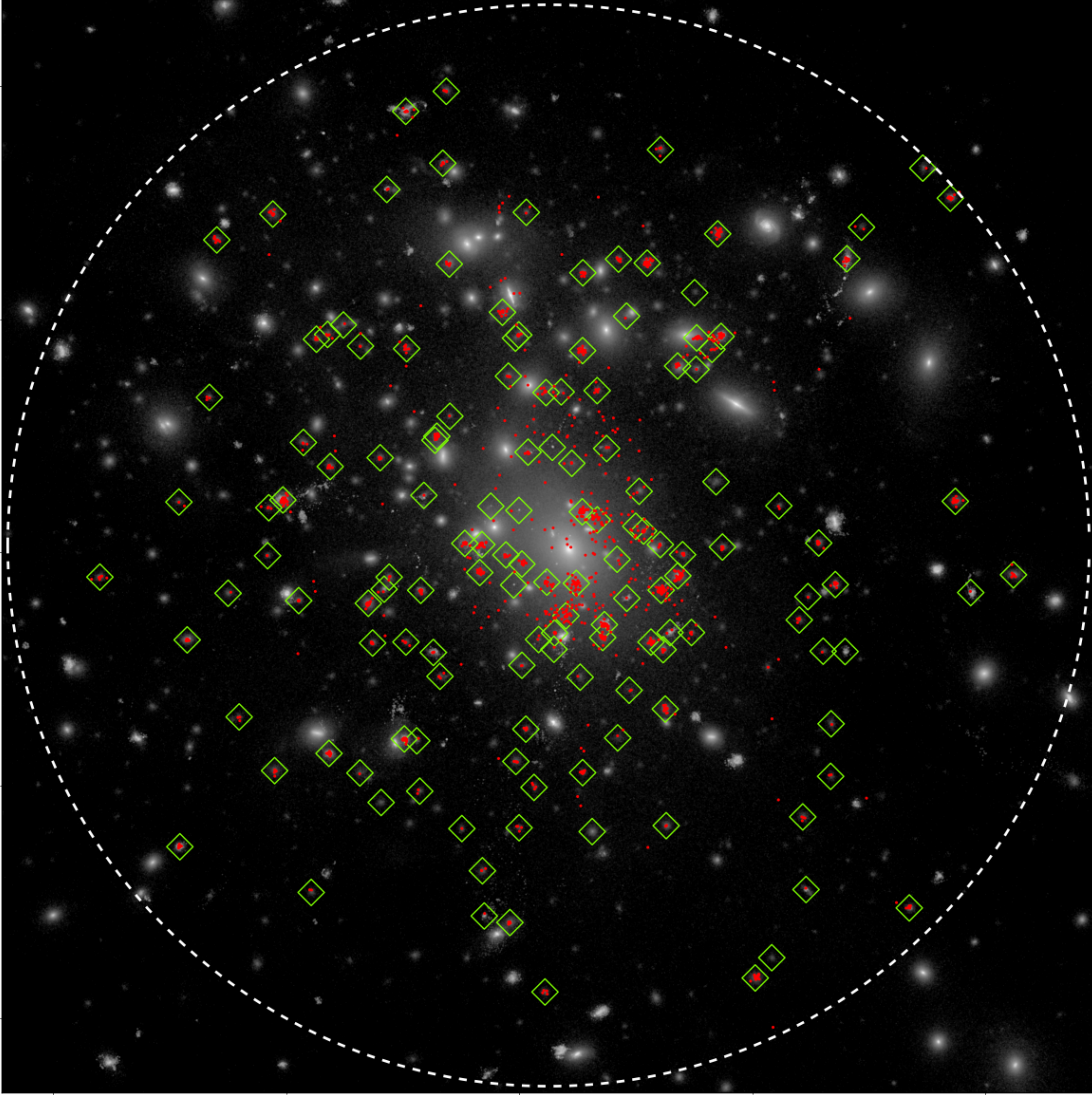
where it was born. In order to approximate the aperture used in studies of the Virgo cluster (Jordan et al. 2007b; Peng et al. 2008), we use  $r_{\text{cut}} = 8$  kpc, but have also checked that apertures in the range 5–10 kpc yield similar results. For field dwarfs (not exposed to stripping) the tagging is not necessary, and we simply do the spatial sampling once at  $t_{\text{max}}$  and check for the number of GCs within the aperture. In order to average-out the results of a particular random realization, we repeated the tagging exercise 10 times for each dwarf and assigned the final  $T_N$  based on the average of these 10 realizations.

Fig. 11 shows the final specific frequency of GCs,  $T_N$ , predicted by our model using all massive GCs with mass above  $M = 4 \times 10^5 M_\odot$  (this mass cut-off is not important, but was chosen to agree roughly with the average normalization of observed GC frequencies in dwarfs). We show the predicted  $T_N$  as a function of stellar mass for the sample of cluster (solid colored dots) and field (black crosses) dwarfs. We find a clear excess of GCs for cluster dwarfs, even after accounting for tidal stripping within the host clusters, with the median  $T_N$  of cluster dwarfs about  $\sim 1.65$  times larger than dwarfs in the field. Most importantly, we find a clear correlation between this GC excess and the “starburstiness” of the star-formation histories in the dwarfs, as shown by the color coding of the dots: cluster dwarfs with clear peaks in their star formation histories (larger  $\sigma_{\text{SFR}}$ ) preferentially dominate the tail of high GC frequencies, whereas dwarfs with a more quiet star formation history tend to show  $T_N$  closer to those of field dwarfs. We therefore see that the combination of early star formation plus the starburst events associated with infall and pericentric passages for cluster dwarfs can account for the more numerous GC populations observed for dEs.

Observationally, much of the excess in GC specific frequency comes from nucleated dEs whereas non-nucleated dEs have GC frequencies more similar to those of dIrrs (Miller et al. 1998; Miller & Lotz 2007). Although our numerical resolution is not sufficient to address the morphology of the simulated dwarfs, the correlation between high  $T_N$  and the presence of starbursts suggests that nucleated dEs are simply the tail of the distribution of dwarf galaxies where environment caused the strongest bursts of star-formation associated with infall and pericentric passages, in agreement with the proposal of Miller & Lotz (2007). Moreover, the excess in  $T_N$  found in Fig. 11 is dominated by dwarfs located in the inner regions of the clusters. The magenta line shows the median specific frequency of GCs for dwarfs with  $r < 0.3r_{200}$  which is a factor  $\sim 1.5$  larger than that of cluster dwarfs in the outskirts  $r > 0.7r_{200}$  (cyan curve) and dwarfs in the field (dashed black curve). This radial dependence is in agreement with the observed trend for dEs in the Virgo cluster (Peng et al. 2008).

The effects of tidal stripping can be significant, but is not enough to erase the initial difference (Fig. 10) expected from our calculation of the mass in GCs. Fig. 12 shows a more comprehensive view of the final distribution of GCs (red dots) with respect to the dwarfs (green squares) within a galaxy cluster (in this case, the most massive of our host clusters). The image shows a luminosity-weighted stellar mass map and indicates that although the majority of GCs are still bound to the dwarfs in which they were born, there are several that have been stripped by the cluster potential and may now belong to the background population of GCs of the massive central galaxy in the cluster. Dwarf elliptical galaxies seem then able to contribute a fair number of “accreted” GCs to the central potential of the host cluster. Moreover, tidally disrupted and unre-





**Figure 12.** Final distribution of tagged GCs (red dots) overlaid on the projected stellar-mass map of our most massive cluster. Dwarf galaxies in this cluster (the only contributors of GCs in this figure) are highlighted with green squares. Although most of the GCs remain bound to the dwarfs where they formed, several of them have been tidally stripped from their native dwarf galaxy, particularly in the inner regions of the cluster where tidal forces are stronger. The stellar content and phase-space properties (positions and velocities) of such stripped GCs could still retain information of their dwarf progenitors, such as orbits, star-formation histories and also help determine the tidal radii of cluster dwarfs.

solved GCs will contribute to the diffuse intra-cluster light instead, a study of which we defer to future work.

The results of this section are encouraging, but we emphasize the limitations of our model. One strong assumption we have made is that the star cluster efficiency  $\Gamma$  scales, *at all redshifts* and for low mass galaxies as the one considered here, with the density of star formation as indicated by Eq. 2. The equation is a power-law fit to observations in nearby star-forming galaxies, and it is not guaranteed that the same relation holds at higher redshifts. In order to explore alternative parametrizations of  $\Gamma$ , we considered the theoretical models presented in [Kruijssen \(2012\)](#), which are based on physical properties of the gas and therefore can be applied at any given time. In this model,  $\Gamma$  scales with the surface density of the gas  $\Sigma_g$ , which we can measure from our simulations.

Although the [Kruijssen](#) model is more detailed than our numerical resolution allows (it requires measurements for the stability

parameter  $Q$  for galaxy disks, among other factors), using standard values of  $Q = 1.5$ , we were able to reproduce the factor  $\sim 2$  relative excess in GC mass for dwarfs in clusters compared to the field<sup>3</sup>. Additionally, we have checked that our definition of size used to compute  $\Sigma_{\text{SFR}}$  in Eq. 2 does not change the results we presented. To do this we vary the definition of size using: the radius enclosing 95% of the star forming gas (the proposed model), half-mass radius of the stars and half-mass radius of the gas, and in all cases recover the *relative* difference between cluster and field dwarfs presented in Fig. 11.

A second important assumption in our model is that the destruction of massive GCs is similar for dwarfs in clusters and

<sup>3</sup> We thank the author for making the code to compute GC efficiency publicly available at <http://www.mpa-garching.mpg.de/cfe>.



in the field. However, for massive GCs, dynamical friction (DF) forces can accelerate their orbital decay, eventually causing them to merge with the host galaxy. Analytical estimates of time needed for GCs to sink to the center of their hosts due to DF can vary from 1-10 Gyr depending on GC mass for a host dwarf galaxy with  $M_* \sim 10^9 M_\odot$  (see fig. 19 in Turner et al. 2012). This indicates that the magnitude of the GC excess in cluster dwarfs can be overestimated in our model. Nonetheless, the net effect of DF is far from clear. For example, the DF timescale depends strongly on the (unknown) initial distribution of the GCs and also on the dark matter density profile of the dwarfs. Halos with lower central densities or constant dark matter cores show much longer DF timescales (Hernandez & Gilmore 1998; Cole et al. 2012). Because tidal stripping of the dark matter halo in satellite dwarfs will tend to lower the central densities (e.g. Hayashi et al. 2003), the sinking of GCs in cluster dwarfs could result, overall, less efficient than in the field. Therefore, although some of the most massive GCs in cluster dwarfs may merge with their hosts, due to the steep mass function of GCs favoring *in number* lower mass GCs, the GCs frequency in cluster dwarfs is likely to remain significantly enhanced with respect to the field.

Finally, we also tested the effects of assuming a shallower GC radial distribution (and thus more prone to tidal stripping for cluster dwarfs). Following observational results by Beasley et al. (2009), we assumed  $\rho \propto r^{-2}$  (instead of the steeper  $-3.5$  slope found in the Milky Way) and sample the position of GCs within a maximum radius of 5 kpc. This cut-off was chosen such that the radius containing half of the GCs is  $\sim 1$ -2 kpc as observed for dwarfs. We repeated the particle tagging step and check for the number of GCs that remained bound to their host dwarfs, as before. We find that although some cluster dwarfs are stripped more easily of their GCs, the majority of the sample manages to retain most of their GCs, suggesting that our result in Fig. 11 is robust to changes in the radial distribution of GCs that are within observational constraints (see also Smith et al. 2013).

We conclude that the model is not overly sensitive to the arbitrary choices we have adopted and that it represents an attractive tool for studying the formation of GCs in cosmological simulations of galaxies where the resolution is not adequate to describe the scale of individual star clusters. The application of this model to our sample of dwarf galaxies indicates that dwarf ellipticals in clusters would naturally have an enhanced frequency of GCs compared to field dwarfs, an effect that is most prominent for dwarfs in the inner parts of clusters; and that such a difference is not only a reflection of an early assembly but is also due to the starburst events associated with infall into the host cluster.

## 6 SUMMARY & CONCLUSION

We use the Illustris simulation to study the formation of dwarf galaxies in clusters. We select 12 host galaxy clusters in the virial mass range  $M_{200} = 0.72$ - $2.32 \times 10^{14} M_\odot$ , with the high mass end akin to systems like the Virgo and Fornax clusters. Dwarf galaxies are selected to be within the virial radii of these clusters at  $z = 0$  and have stellar masses in the range  $M_* = 3 \times 10^8$ - $1 \times 10^{10} M_\odot$ . We find 1071 candidate dwarfs that satisfy our selection criteria. We construct an equal-number control sample of field dwarfs selected in the same stellar mass range at  $z = 0$  but that are central objects of their FoF group. Our main findings can be summarized as follows:

- At  $z = 0$  the population of dwarfs in clusters has redder colors

and lower star formation rates than field objects, in good agreement with the properties of observed dEs. The parameters in the simulation were not tuned to reproduce this, so this is a successful prediction of our model that motivates further studies into the evolution that shaped these two different populations.

- Dwarfs in clusters are mostly genuine low mass objects and not the descendants of more massive galaxies that have been substantially stripped. Only 14% of our dwarfs have lost more than 50% of their stellar mass due to tidal effects.

- Although by construction both samples have the same stellar mass at  $z = 0$ , the assembly of cluster and field dwarfs is remarkably different: cluster dwarfs form their stars at earlier times and at higher star formation rates compared to field dwarfs. Because of this difference in the build-up times, the progenitors of dwarfs that are in clusters today were, at the average infall time of the sample  $z \sim 1$ , about 3.5 times more massive than the progenitors of today's field dwarfs at the same time.

- The star formation histories of dwarfs in clusters often show significant starburst events which are not present in the population of field dwarfs. These starbursts are associated with infall and/or first pericentric passages, likely due to gas compression in the dwarfs under the combined effects of tidal and ram-pressure forces.

- The cessation of star formation in cluster dwarfs occurs within timescales (median)  $\sim 3$ -5.5 Gyr after they become satellite galaxies. We find a positive trend with mass, in which low mass dwarfs go quiescent most rapidly. Nevertheless, there is a large scatter around these median values, with differences  $\geq 7$  Gyr at the same  $M_*$ . This highlights the varied paths by which star formation is halted: dwarfs with significant starburst events quench rapidly, whereas others in the sample simply consume their gas fuel and quench over much longer timescales.

- The different star formation histories of cluster and field dwarfs can have a significant impact on their populations of globular clusters. To study this, we implement a post-processing model of GC formation and apply it to our sample of cluster and field dwarfs. In a scenario where: *a*) GCs are the evolved population of young star clusters and *b*) the fraction of stars born in clusters compared to field stars scales with either the star formation density or gas density, our results indicate that dwarfs living in galaxy clusters today should have an enhanced number of globular clusters per unit stellar mass compared to galaxies in the field with similar stellar mass, in agreement with observations. After accounting for stripping, we find that the difference in the mean specific frequency of GCs,  $T_N$ , is a factor  $\sim 1.6$ , with extreme cases having  $T_N$  as much as 10 times larger than the field dwarf population.

Our results lend support to the notion that dEs in clusters share a similar origin with isolated dIrr galaxies in the field, but their properties have been fundamentally altered due to the cluster environment. This idea, although perhaps the most popular scenario for the formation of dEs, appeared to be in tension with a larger specific frequency of GCs observed for cluster dwarfs. Here we find that such a trend could arise from the different star formation histories of the samples.

We emphasize, however, that the *progenitors* of cluster and field dwarfs of similar mass at  $z = 0$  can differ substantially in their masses at earlier times. Observational studies that are seeking to find a population of isolated dwarfs with the same *progenitors* as dwarfs in clusters today, may need to focus on present-day gas-rich galaxies that are  $\sim 3$  times more massive than the target dE population. This difference corresponds to the freeze-out of star formation that occurs for cluster dwarfs after infall, while the analog field

population can continue to form stars at a normal rate outgrowing their cluster peers from  $z \sim 1$  until now.

The results presented here have a number of predictions that can be tested observationally. For example, in our simulations a significant number of cluster dwarfs show intense starburst episodes, the majority of which are then followed by a rapid shut-off of star formation. Such events will leave a clear imprint in the stellar populations of cluster dwarfs, likely with  $\alpha$ -element enhancements compared to dwarfs in the field where star formation proceeded more slowly. Such a trend could be seen in observations when detailed metallicity data becomes available for dEs in nearby clusters.

Another interesting prediction pertains to the kinematics of GCs around dEs. Our modeling of GCs suggests that some of the native GCs in dwarfs may have been stripped (or are in the process of being stripped) by the host potential. These stripped GCs will retain information about their origin imprinted in their phase-space properties (positions and velocities) that could be used to design observational strategies to identify the full population of native GCs born in dE galaxies.

Finally, current and upcoming observations provide valuable insight into the structural properties of cluster dwarfs. Results so far have revealed a fascinating variety, with dEs showing little or no rotation, well defined but faded disks, and even counter-rotating components (Toloba et al 2014a,b). Moreover, dEs in the Local Group are also starting to show interesting differences in their star formation histories that could be linked to their different orbits (Geha et al. 2015). In a follow-up study, we will focus on the analysis of zoom-in simulations of clusters that have the resolution needed to address the morphological transformation of dwarfs in clusters. This will provide a comprehensive theoretical view of the evolutionary link between dEs and their suspected dIrr progenitors and the many paths that have helped to shape this dichotomy in the dwarf galaxy population.

## ACKNOWLEDGEMENTS

The authors are grateful to Mario Abadi, James Bullock, Mike Cooper, Raja Guhathakurtha, Julio Navarro, Diederik Kruijssen, Eric Peng, Elisa Toloba and Carlos Vera-Ciro for insightful and stimulating discussions. We would like to thank Shy Genel, Debora Sijacki and Volker Springel for early access to the simulations and comments on the draft. We would like to thank the referee, Hugo Martel, for helpful comments that improved the manuscript. Simulations were run on the Harvard Odyssey and CfA/ITC clusters, the Ranger and Stampede supercomputers at the Texas Advanced Computing Center as part of XSEDE, the Kraken supercomputer at Oak Ridge National Laboratory as part of XSEDE, the CURIE supercomputer at CEA/France as part of PRACE project RA0844, and the SuperMUC computer at the Leibniz Computing Centre, Germany, as part of project pr85je. L.H. acknowledges support from NASA grant NNX12AC67G and NSF grant AST-1312095. AP acknowledges support from the HST grant HST-AR-13897.

## REFERENCES

Adamo A., Östlin G., Zackrisson E., 2011, *MNRAS*, 417, 1904  
 Adamo A., Östlin G., Zackrisson E., Hayes M., Cumming R. J., Micheva G., 2010, *MNRAS*, 407, 870  
 Barnes J. E., Hernquist L., 1996, *ApJ*, 471, 115

Beasley M. A., Cenarro A. J., Strader J., Brodie J. P., 2009, *AJ*, 137, 5146  
 Besla G., Kallivayalil N., Hernquist L., Robertson B., Cox T. J., van der Marel R. P., Alcock C., 2007, *ApJ*, 668, 949  
 Besla G., Kallivayalil N., Hernquist L., van der Marel R. P., Cox T. J., Kereš D., 2010, *ApJL*, 721, L97  
 Besla G., Kallivayalil N., Hernquist L., van der Marel R. P., Cox T. J., Kereš D., 2012, *MNRAS*, 421, 2109  
 Binggeli B., Tarenghi M., Sandage A., 1990, *A&A*, 228, 42  
 Böhringer H., Briel U. G., Schwarz R. A., Voges W., Hartner G., Trümper J., 1994, *Nature*, 368, 828  
 Boselli A., Boissier S., Cortese L., Gavazzi G., 2008, *ApJ*, 674, 742  
 Bournaud F., Duc P.-A., Emsellem E., 2008, *MNRAS*, 389, L8  
 Cole D. R., Dehnen W., Read J. I., Wilkinson M. I., 2012, *MNRAS*, 426, 601  
 Conselice C. J., Gallagher III J. S., Wyse R. F. G., 2003, *AJ*, 125, 66  
 Cooper A. P., Cole S., Frenk C. S., White S. D. M., Helly J., Benson A. J., De Lucia G., Helmi A., Jenkins A., Navarro J. F., Springel V., Wang J., 2010, *MNRAS*, 406, 744  
 Cooper A. P., D’Souza R., Kauffmann G., Wang J., Boylan-Kolchin M., Guo Q., Frenk C. S., White S. D. M., 2013, *MNRAS*, 434, 3348  
 Cooper A. P., Gao L., Guo Q., Frenk C. S., Jenkins A., Springel V., White S. D. M., 2015, *MNRAS*, 451, 2703  
 Davis M., Efstathiou G., Frenk C. S., White S. D. M., 1985, *ApJ*, 292, 371  
 de Grijs R., Smith L. J., Bunker A., Sharp R. G., Gallagher J. S., Anders P., Lançon A., O’Connell R. W., Parry I. R., 2004, *MNRAS*, 352, 263  
 de Rijcke S., Michielsen D., Buyle P., Zeilinger W. W., Dejonghe H., Hau G. K. T., 2005, *Astronomische Nachrichten*, 326, 489  
 Dekel A., Silk J., 1986, *ApJ*, 303, 39  
 Di Matteo T., Springel V., Hernquist L., 2005, *Nature*, 433, 604  
 Dolag K., Borgani S., Murante G., Springel V., 2009, *MNRAS*, 399, 497  
 D’Onghia E., Besla G., Cox T. J., Hernquist L., 2009, *Nature*, 460, 605  
 Dressler A., 1980, *ApJ*, 236, 351  
 Elmegreen B. G., Efremov Y. N., 1997, *ApJ*, 480, 235  
 Faucher-Giguère C.-A., Lidz A., Zaldarriaga M., Hernquist L., 2009, *ApJ*, 703, 1416  
 Fillingham S. P., Cooper M. C., Wheeler C., Garrison-Kimmel S., Boylan-Kolchin M., Bullock J. S., 2015, *ArXiv e-prints*  
 Font A. S., Bower R. G., McCarthy I. G., Benson A. J., Frenk C. S., Helly J. C., Lacey C. G., Baugh C. M., Cole S., 2008, *MNRAS*, 389, 1619  
 Geha M., Blanton M. R., Yan R., Tinker J. L., 2012, *ApJ*, 757, 85  
 Geha M., Guhathakurta P., van der Marel R. P., 2002, *AJ*, 124, 3073  
 Geha M., Weisz D., Grocholski A., Dolphin A., van der Marel R. P., Guhathakurta P., 2015, *ApJ*, 811, 114  
 Genel S., Fall S. M., Hernquist L., Vogelsberger M., Snyder G. F., Rodriguez-Gomez V., Sijacki D., Springel V., 2015, *ApJL*, 804, L40  
 Genel S., Vogelsberger M., Nelson D., Sijacki D., Springel V., Hernquist L., 2013, *MNRAS*, 435, 1426  
 Genel S., Vogelsberger M., Springel V., Sijacki D., Nelson D., Snyder G., Rodriguez-Gomez V., Torrey P., Hernquist L., 2014, *MNRAS*, 445, 175  
 Georgiev I. Y., Hilker M., Puzia T. H., Goudfrooij P., Baumgardt

- H., 2009, MNRAS, 396, 1075
- Gnedin O. Y., 2003, ApJ, 582, 141
- Goddard Q. E., Bastian N., Kennicutt R. C., 2010, MNRAS, 405, 857
- Grebel E. K., 1999, in Whitelock P., Cannon R., eds, The Stellar Content of Local Group Galaxies Vol. 192 of IAU Symposium, Evolutionary Histories of Dwarf Galaxies in the Local Group. p. 17
- Griffen B. F., Drinkwater M. J., Thomas P. A., Helly J. C., Pimbblet K. A., 2010, MNRAS, 405, 375
- Guo Q., White S., Boylan-Kolchin M., De Lucia G., Kauffmann G., Lemson G., Li C., Springel V., Weinmann S., 2011, MNRAS, 413, 101
- Harris W. E., 1996, VizieR Online Data Catalog, 7195, 0
- Harris W. E., Pudritz R. E., 1994, ApJ, 429, 177
- Hayashi E., Navarro J. F., Taylor J. E., Stadel J., Quinn T., 2003, ApJ, 584, 541
- Hernandez X., Gilmore G., 1998, MNRAS, 297, 517
- Hernquist L., Katz N., 1989, ApJS, 70, 419
- Ho L. C., Filippenko A. V., 1996, ApJ, 472, 600
- Janz J., Laurikainen E., Lisker T., Salo H., Peletier R. F., Niemi S.-M., den Brok M., Toloba E., Falcón-Barroso J., Boselli A., Hensler G., 2012, ApJL, 745, L24
- Jordán A., McLaughlin D. E., Côté P., Ferrarese L., Peng E. W., Mei S., Villegas D., Merritt D., Tonry J. L., West M. J., 2007, ApJS, 171, 101
- Katz N., Weinberg D. H., Hernquist L., 1996, ApJS, 105, 19
- Kauffmann G., White S. D. M., Heckman T. M., Ménard B., Brinchmann J., Charlot S., Tremonti C., Brinkmann J., 2004, MNRAS, 353, 713
- Kravtsov A. V., Gnedin O. Y., 2005, ApJ, 623, 650
- Kruijssen J. M. D., 2012, MNRAS, 426, 3008
- Kruijssen J. M. D., Cooper A. P., 2012, MNRAS, 420, 340
- Laporte N., Pelló R., Hayes M., Schaerer D., Boone F., Richard J., Le Borgne J. F., Kneib J. P., Combes F., 2012, A&A, 542, L31
- Lelli F., Fraternali F., Verheijen M., 2014, A&A, 563, A27
- Lisker T., 2009, Astronomische Nachrichten, 330, 1043
- Lisker T., Grebel E. K., Binggeli B., 2006, AJ, 132, 497
- Lisker T., Weinmann S. M., Janz J., Meyer H. T., 2013, MNRAS, 432, 1162
- Martínez H. J., Zandivarez A., Domínguez M., Merchán M. E., Lambas D. G., 2002, MNRAS, 333, L31
- Mayer L., Governato F., Colpi M., Moore B., Quinn T., Wadsley J., Stadel J., Lake G., 2001, ApJL, 547, L123
- Mengel S., Lehnert M. D., Thatte N., Genzel R., 2002, A&A, 383, 137
- Mihos J. C., Hernquist L., 1996, ApJ, 464, 641
- Miller B. W., Lotz J. M., 2007, ApJ, 670, 1074
- Miller B. W., Lotz J. M., Ferguson H. C., Stiavelli M., Whitmore B. C., 1998, ApJL, 508, L133
- Napolitano N. R., Pannella M., Arnaboldi M., Gerhard O., Aguerri J. A. L., Freeman K. C., Capaccioli M., Ghigna S., Governato F., Quinn T., Stadel J., 2003, ApJ, 594, 172
- Nelson D., Pillepich A., Genel S., Vogelsberger M., Springel V., Torrey P., Rodríguez-Gomez V., Sijacki D., Snyder G. F., Griffen B., Marinacci F., Blecha L., Sales L., Xu D., Hernquist L., 2015, ArXiv e-prints
- Nelson D., Vogelsberger M., Genel S., Sijacki D., Kereš D., Springel V., Hernquist L., 2013, MNRAS, 429, 3353
- Peñarrubia J., Navarro J. F., McConnachie A. W., 2008, Astronomische Nachrichten, 329, 934
- Peng E. W., Jordán A., Côté P., Takamiya M., West M. J., Blakeslee J. P., Chen C.-W., Ferrarese L., Mei S., Tonry J. L., West A. A., 2008, ApJ, 681, 197
- Prieto J. L., Gnedin O. Y., 2008, ApJ, 689, 919
- Ramos F., Coenda V., Muriel H., Abadi M., 2015, ApJ, 806, 242
- Renaud F., Boily C. M., Fleck J.-J., Naab T., Theis C., 2008, MNRAS, 391, L98
- Rodríguez-Gomez V., Genel S., Vogelsberger M., Sijacki D., Pillepich A., Sales L. V., Torrey P., Snyder G., Nelson D., Springel V., Ma C.-P., Hernquist L., 2015, MNRAS, 449, 49
- Ryś A., Falcón-Barroso J., van de Ven G., 2013, MNRAS, 428, 2980
- Sabatini S., Davies J., van Driel W., Baes M., Roberts S., Smith R., Linder S., O’Neil K., 2005, MNRAS, 357, 819
- Sales L. V., Vogelsberger M., Genel S., Torrey P., Nelson D., Rodríguez-Gomez V., Wang W., Pillepich A., Sijacki D., Springel V., Hernquist L., 2015, MNRAS, 447, L6
- Sánchez-Janssen R., Aguerri J. A. L., 2012, MNRAS, 424, 2614
- Shapiro K. L., Genzel R., Förster Schreiber N. M., 2010, MNRAS, 403, L36
- Sijacki D., Springel V., Di Matteo T., Hernquist L., 2007, MNRAS, 380, 877
- Sijacki D., Vogelsberger M., Kereš D., Springel V., Hernquist L., 2012, MNRAS, 424, 2999
- Silva-Villa E., Larsen S. S., 2011, A&A, 529, A25
- Smith R., Davies J. I., Nelson A. H., 2010, MNRAS, 405, 1723
- Smith R., Sánchez-Janssen R., Fellhauer M., Puzia T. H., Aguerri J. A. L., Farias J. P., 2013, MNRAS, 429, 1066
- Snyder G. F., Torrey P., Lotz J. M., Genel S., McBride C. K., Vogelsberger M., Pillepich A., Nelson D., Sales L. V., Sijacki D., Hernquist L., Springel V., 2015, ArXiv e-prints
- Springel V., 2005, MNRAS, 364, 1105
- Springel V., 2010, MNRAS, 401, 791
- Springel V., Di Matteo T., Hernquist L., 2005, MNRAS, 361, 776
- Springel V., Hernquist L., 2003, MNRAS, 339, 289
- Springel V., White S. D. M., Jenkins A., Frenk C. S., Yoshida N., Gao L., Navarro J., Thacker R., Croton D., Helly J., Peacock J. A., Cole S., Thomas P., Couchman H., Evrard A., Colberg J., Pearce F., 2005, Nature, 435, 629
- Springel V., Yoshida N., White S. D. M., 2001, New Astronomy, 6, 79
- Toloba E., Guhathakurta P., Peletier R. F., et al. 2014, ApJS, 215, 17
- Toloba E., Guhathakurta P., van de Ven G., et al. 2014, ApJ, 783, 120
- Torrey P., Vogelsberger M., Genel S., Sijacki D., Springel V., Hernquist L., 2014, MNRAS, 438, 1985
- Turner M. L., Côté P., Ferrarese L., Jordán A., Blakeslee J. P., Mei S., Peng E. W., West M. J., 2012, ApJS, 203, 5
- van Zee L., Barton E. J., Skillman E. D., 2004, AJ, 128, 2797
- van Zee L., Skillman E. D., Haynes M. P., 2004, AJ, 128, 121
- Vogelsberger M., Genel S., Sijacki D., Torrey P., Springel V., Hernquist L., 2013, MNRAS, 436, 3031
- Vogelsberger M., Genel S., Springel V., Torrey P., Sijacki D., Xu D., Snyder G., Bird S., Nelson D., Hernquist L., 2014, Nature, 509, 177
- Vogelsberger M., Genel S., Springel V., Torrey P., Sijacki D., Xu D., Snyder G., Nelson D., Hernquist L., 2014, MNRAS, 444, 1518
- Vogelsberger M., Sijacki D., Kereš D., Springel V., Hernquist L., 2012, MNRAS, 425, 3024
- Wang L., Li C., Kauffmann G., De Lucia G., 2007, MNRAS, 377, 1419

- Wang W., Sales L. V., Henriques B. M. B., White S. D. M., 2014, MNRAS, 442, 1363
- Wetzel A. R., Tinker J. L., Conroy C., van den Bosch F. C., 2013, MNRAS, 432, 336
- Wheeler C., Phillips J. I., Cooper M. C., Boylan-Kolchin M., Bullock J. S., 2014, MNRAS, 442, 1396
- Yang X., Mo H. J., van den Bosch F. C., 2009, ApJ, 695, 900
- Zepf S. E., Ashman K. M., 1993, MNRAS, 264, 611